Catalysis Letters (2019) 149:100–106
https://doi.org/10.1007/s10562-018-2585-z

Nanostructured Potassium-Manganese Oxides Decorated with Pd Nanoparticles as Efficient Catalysts for Low-Temperature Soot Oxidation

Tomasz Jakubek[1] · Kathryn Ralphs[2] · Andrzej Kotarba[1] · Haresh Manyar[2]

Received: 7 August 2018 / Accepted: 4 October 2018 / Published online: 11 October 2018

Abstract
Two nanostructured potassium–manganese oxides, with a layered (OL) and tunneled structure (OMS-2), were synthesized and their surface decorated with 1% Pd. All prepared samples were characterized by means of X-ray diffraction, Raman spectroscopy, N_2-BET specific surface area analysis, TPR, SEM/TEM. Catalytic activity in soot combustion in different reaction conditions was investigated (*tight* contact, *loose* contact, *loose* contact with NO addition). The obtained results revealed, that manganese oxides are highly catalytically active in soot combustion, shifting the reaction temperature window by 280 °C for OMS-2 and 300 °C for OL in comparison to the non-catalytic process. Furthermore, Pd promotion is beneficial in all cases, lowering the window of soot combustion compared to the unpromoted oxides, with the most significant effect for *loose* contact conditions. The difference in activity between tight and loose contacts can be successfully bridged in the presence of NO due to its transformation into NO_2. The particular activity of 1% Pd/OMS-2 and 1% Pd/OL pave the road for their further development towards catalytic system for efficient soot removal in the conditions present in diesel exhaust gases.

Graphical Abstract

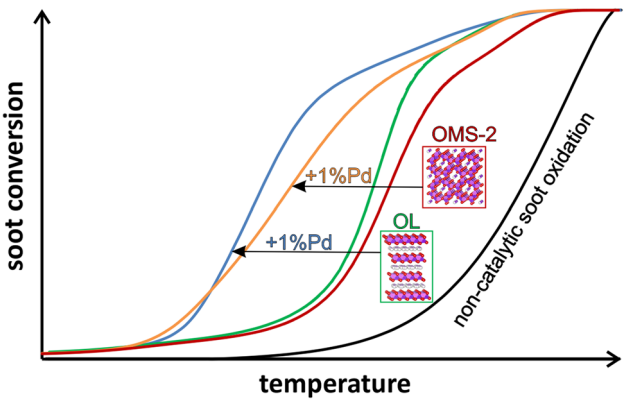

Keywords Palladium supported on potassium–manganese oxides · OMS-2 · OL · Soot combustion · Diesel exhaust

1 Introduction

One common way to produce energy is the burning of carbon fuels. In ideal conditions the only products are water and CO_2. Unfortunately, in most mobile and stationary sources it is impossible to maintain ideal conditions, implying by-products formation, usually of a pollutant nature. One such

✉ Andrzej Kotarba
kotarba@chemia.uj.edu.pl

✉ Haresh Manyar
h.manyar@qub.ac.uk

Extended author information available on the last page of the article

source of pollutants are exhaust gases of diesel engines. Unfortunately, apart from numerous advantages, these engines have a large defect in the form of high emissions of nitrogen oxides (NOx) and particulate matter (PM). Soot nanoparticles formed during diesel engine operation are harmful for the environment, contributing to the greenhouse effect, but more importantly are highly hazardous for human health being both carcino- and mutagenic [1, 2]. Thus, emission thresholds were introduced and are being continuously tightened in the industrialized countries.

The use of diesel particulate filters (DPF's), which is permeable to gases but not to solid fractions, can lower PM emission by up to 99%. The channeled filter typically has every second channel plugged on one side, at the source, with the other half of the channels plugged on the exit. This forces the gas to pass through the porous walls, leaving the particulate matter behind. Soot accumulated on the filter is burned either continuously or periodically in order to reduce the pressure drop and to increase the ability to trap additional PM. In order to burn the trapped soot a temperature of 600 °C is required, which is not available during normal engine operation and different methods must be used to artificially raise the temperature (post injection), or the channels can be coated with catalytically active materials, which can continuously regenerate DPFs in the temperature of exhaust gasses [3]. However, the efficiency of catalytically coated diesel particulate filters (CDPF) is related the tight contact between the soot molecules and the catalyst, whereas under practical conditions loose contact mostly predominates [4]. Thus, many of the catalysts tested in laboratory conditions in soot oxidation reactions are known to exhibit rather limited performance upon real driving scenarios.

A variety of catalytic materials, mainly transition metal oxides [5–9], spinels [10, 11], perovskites [12], mixed metal oxides [13, 14] and supported noble metals were reported to be active in soot oxidation [6, 15, 16]. Furthermore, promotion by alkali metals is reported to increase the catalysts ability to activate oxygen (by lowering the work function of the catalysts surface) as well as to form compounds with low melting point temperatures. This is meant to increase the number of contact points between the catalyst surface and soot particles, which is essential for soot oxidation [17–20]. The class of compounds investigated in this context are mixed oxides built of d-metal cations (Fe, Mn, Co), which works as a redox center, and an alkali cation, most often potassium [21]. The combination of these elements can lead to the formation of nanostructured materials, where alkali cations are located in the tunnels or layers.

Cryptomelane (Fig. 1a) is a nanoscale alkali doped manganese octahedral molecular sieve (OMS-2). The high activity in oxidation reactions of Mn-based nanostructured materials is well known in heterogeneous catalysis [22–26]. Cryptomelane is a Hollandite type manganese oxide, with a

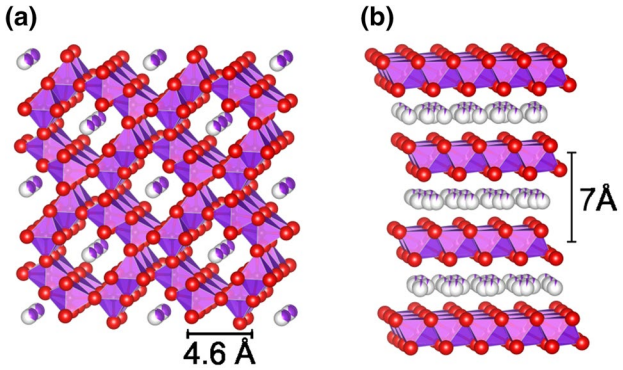

Fig. 1 Structures of the investigated supports: OMS-2 (**a**) and OL (**b**)

tunnelled structure (OMS-2) nanostructured by alkali. The tunnels are built up of four double-wide (2 × 2) slabs of octahedral MnO_6 units, connected by edges, forming tunnel dimensions of 4.6 × 4.6 Å [27]. Similarly, octahedral layered birnessite (OL-1) is formed from edge-sharing MnO_6 octahedral units forming a two-dimensional (2D) layered structure (Fig. 1b). The layers can contain different exchangeable cations (e.g. K^+) as well as molecules in the interlayer space (7 Å) [28]. Their high reactivity can be assigned to a combination of several features, such as beneficial porous structure, redox properties due to the mixed valence framework, and high oxygen mobility [29–32].

The aim of this work is to explore the synergistic effects between the potassium containing manganese oxide support and palladium nanoparticles for designing an efficient catalyst for low temperature soot oxidation. The two investigated ternary oxide supports both contain potassium and manganese cations in either a tunneled or layered nanostructure, on which the Pd nanoparticles are dispersed. Furthermore, the effect of NO, which is present in the diesel gas stream, is evaluated as an effective way to transfer oxygen (in the form of NO_2) from the catalyst to soot particles, bridging tight and loose contact conditions.

2 Experimental

2.1 Catalyst Preparation

OMS-2 materials were prepared by a modified sol gel method, first developed by Duan et al. [33]. In a typical preparation, 12.65 g $KMnO_4$ (0.08 mol; Alfa Aesar) were dissolved in 800 ml deionized water at room temperature and stirred with an overhead stirrer. To this solution, 3.09 g maleic acid (0.027 mol; Sigma-Aldrich) was gradually added. The resultant mixture was stirred for 1 h. After 1 h the resultant gel was washed four times with deionized water. The gel was then filtered and vacuum dried for 1 h,

before it was transferred to an oven for overnight drying at 110 °C, followed by subsequent calcination in the flow of air at 450 °C for 4 h.

OL materials were prepared by a modified sol gel method [34]. In a typical preparation, 7.49 g $KMnO_4$ (0.05 mol; Alfa Aesar) were dissolved in 150 ml deionized water. A second solution of 0.7 g KOH (0.012 mol; Sigma-Aldrich) dissolved in 50 ml deionized water and 50 ml ethanol. The first solution was added to the second solution and stirred for 1 h. After 1 h, the resultant mixture was transferred to a Teflon reactor and aged at 80 °C in an oven for 48 h. The product was then washed with deionized water until a pH under 9 was achieved. The resultant gel was then dried overnight at 110 °C, followed by subsequent calcination in the flow of air at 400 °C for 2 h.

1% Pd/OMS-2 and 1% Pd/OL was prepared by incipient wetness impregnation using palladium nitrate (assay 39%, Alfa Aesar) as palladium precursor. After impregnation the catalyst was dried at 120 °C for 12 h and calcined at 450 °C for 4 h.

2.2 Physicochemical Characterization

X-ray diffraction measurements were made with CuKα radiation (1.5405 Å) by using a PANalytical X'PERT PRO MPD diffractometer equipped with reflection geometry, a NaI scintillation counter, a curved graphite crystal monochromator and a nickel filter. All measurements were carried out *ex situ* using a spinning stage. The diffractograms were recorded from 5° to 70° with a step size of 0.017°.

The micro-Raman spectra were recorded in ambient conditions using a RenishawInVia spectrometer equipped with a Leica DMLM confocal microscope and a CCD detector, with an excitation wavelength of 785 nm. The laser power at the sample position was 1.5 mW (0.5% of total power) with a magnification of ×20. The Raman scattered light was collected in the spectral range of 100–1000 cm^{-1}. At least six scans, 10 s each, were accumulated to ensure a sufficient signal to noise ratio.

H_2-TPR measurements were performed in a u-shape quartz flow reactor (diameter ca. 5 mm) in the 20–600 °C temperature range. About 0.025 g of sample was used for TPR experiments. All samples were pretreated in a stream of helium for 1 h at a temperature of 120 °C to remove physically adsorbed water. Upon cooling to room temperature, the TPR analysis was performed with a temperature ramp of 10 °C min^{-1} and a reducing gas mixture of 5% H_2 in Ar flowing at 30 cm^3 min^{-1}. The TPR profiles were recorded using a TCD detector.

The surface area, total pore volume and average pore diameter were measured by N_2 adsorption–desorption isotherms at 77 K using Micromeritics ASAP 2020. The pore size was calculated on the adsorption branch of the isotherms using Barrett–Joyner–Helenda (BJH) method and the surface area was calculated using the Brunauer–Emmett–Teller (BET) method. Metal analysis was performed using a Perkin–Elmer Optima 4300 ICP-OES to check the metal loading on Pd supported on OMS-2 and OL catalysts.

SEM images were obtained using a Quanta FEG 250 Scanning Electron Microscope. The samples were prepared sonicating the material for 15 min then mounting on a specimen stub equipped with double sided tape. SEM analysis was then carried out under high vacuum and images of the sample recorded.

TEM images were obtained using a Philips Tecnai F20D spectrometer with a field emission gun. The accelerating voltage was 200 kV and the resolution was 0.2 nm. Samples were prepared by dispersing in methanol and sonicating for 15 min. They were analyzed on holey carbon film copper grids.

Temperature programmed oxidation (TPO) experiments were used to determine the catalytic activity of the received sample. The reactions were performed in both *tight* and *loose contact* conditions. Both reaction mixtures were prepared by weighing 50 mg of the catalyst mixed with soot (Degussa - Printex 80) in an 8:1 ratio. The mixture was then ground for 10 min in an agate mortar (*tight contact*) or shaken in a plastic container for 10 s (*loose contact*). During the experiments a gas mixture consisting of 5% oxygen in He as well as 3.75% O_2, 0.25% NO in He, both at a 60 ml min^{-1} flow was passed through the reactor. The reactor was heated by a ceramic oven from room temperature to 800 °C at a rate of 10 °C min^{-1}. Changes in gas concentrations of the reactants were monitored by a QMS (SRS RGA 200) using the following mass to charge ratios: $m/z = 32$ (O2), $m/z = 44$ (CO_2); 28 (CO); 18 (H_2O) (as well as $m/z = 2$ (H2); 16 (O/O_2) for control purposes). The conversion of soot was calculated by the integration of the QMS signal from CO_2.

3 Results and Discussion

The surface area and pore volumes of the catalysts obtained by BET N_2 isotherm are shown in Table 1. The metal loading of all the catalysts prepared (with the nominal wt%

Table 1 Physical properties of manganese oxide catalysts

Catalyst	Surface area		Metal content (%)		
	BET surface area (m^2 g^{-1})	Pore volume (cm^3 g^{-1})	Pd	K	Mn
OMS-2	104	0.2	0	9.3	62.2
OL	122	0.2	0	10.3	54.4
1% Pd/OMS-2	30	0.09	0.58	8.5	59.1
1% Pd/OL	48	0.1	0.62	9.6	51.4

loadings given in the catalyst descriptor) was determined by ICP-OES analysis (Table 1). The results showed decrease in the surface area of the catalyst after metal deposition, and metal loadings were measured to be on the lower side of the expected 1 wt% loading.

XRD measurements for OMS-2, OL, Pd/OMS-2 and Pd/OL are shown in Fig. 2. The diffractograms showed the materials to be essentially monophasic with no impurities of other manganese oxide forms. It was observed that the calcination in the flow of air after immobilization of Pd nanoparticles to OL induced a partial solid-state phase transition from OL to OMS-2 as evidenced by the appearance of characteristic peaks for OMS-2 (i.e. at 18°) in the XRD pattern for Pd supported on OL.

Raman spectra obtained for investigated samples were shown in Fig. 3. Bands at 186, 285, 393, 479, 514, 582, 639 cm^{-1} were visible on the OMS-2 spectra. The two most intense bands on the OMS-2 spectra, 582 and 639 cm^{-1}, can be assigned to vibrations of the tetragonal structure in the interstitial space of the tunnels. The first is due to the movement of oxygen atoms relative to the manganese atoms along the MnO_6 octahedral chain while the latter are due to the oxygen movement in a perpendicular motion to the chain. The band at 186 cm^{-1} can be assigned to the translational movement of the MnO_6 octahedra, while the band at 393 cm^{-1} can be attributed to the bending vibrations the Mn–O bond. The remaining bands are unassigned in the found literature. On the OL spectra, bands at 280, 409, 477, 506, 577, 634 cm^{-1} are present. The most characteristic bands for birnessite, 634, 577, are due to Mn–O bond of the MnO_6 groups in the interlayer direction and the Mn–O–Mn vibration in the chain framework, respectively. The bands at 280 and 409 cm^{-1} can be assigned to the K–O vibration in the interlayer space while the remaining were unassigned in literature [35–38]. The unpromoted OL differs slightly from Pd/OL, confirming the results of the XRD tests. The

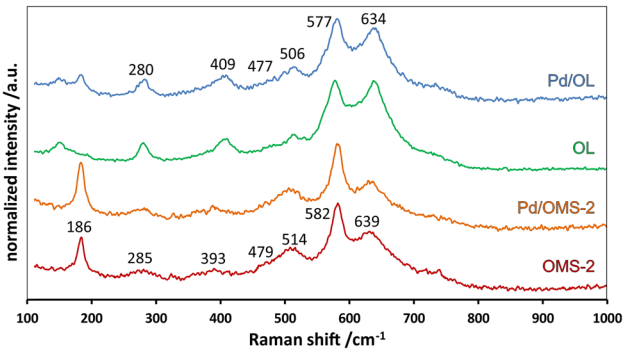

Fig. 3 Raman spectra of tested Pd-doped and undoped OL and OMS-2 catalysts

band near 185 cm^{-1} is shown to appear and the intensity of the band near 577 cm^{-1} is shown to increase in comparison with the band near 639 cm^{-1}, signaling the partial formation of the OMS-2 phase. Both spectra for OMS-2 and Pd/OMS-2 do not differ from one another, in line with the XRD evidence of the structural integrity of OMS-2. A comparison of the effect of Pd deposition on OL and OMS-2 reveals that the noble metal-oxide interaction is much stronger for the layered OL material, resulting in its partial transformation into the tunneled OMS-2.

Temperature programmed reduction in H_2 was performed, with the results presented in Fig. 4. The unpromoted catalysts both gave profiles showing one wide consumption peak with the maxima placed at 429 and 403 °C for OMS-2 and OL, respectively. The broad profile of these maxima can be attributed to the two-step reduction process of the catalysts: $MnO_2 \rightarrow Mn_3O_4$ and further $Mn_3O_4 \rightarrow MnO$ at higher temperature, marked in Fig. 4 by green and blue shadowing, respectively [39]. The addition of Pd results in a more complicated reduction profile. Two peaks for low and high temperature reduction can be easily distinguished, for both

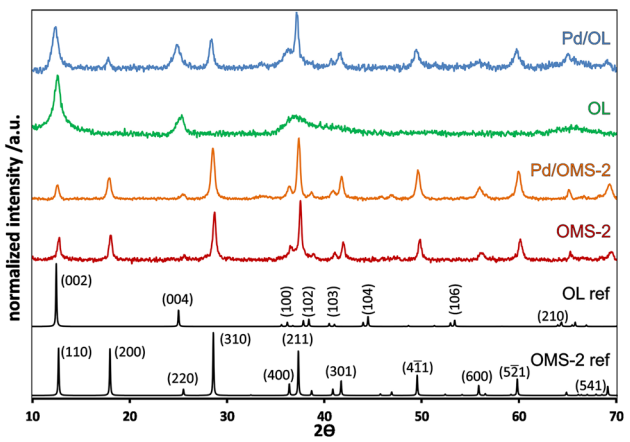

Fig. 2 XRD patterns for OMS-2, OL, Pd/OL and Pd/OMS-2

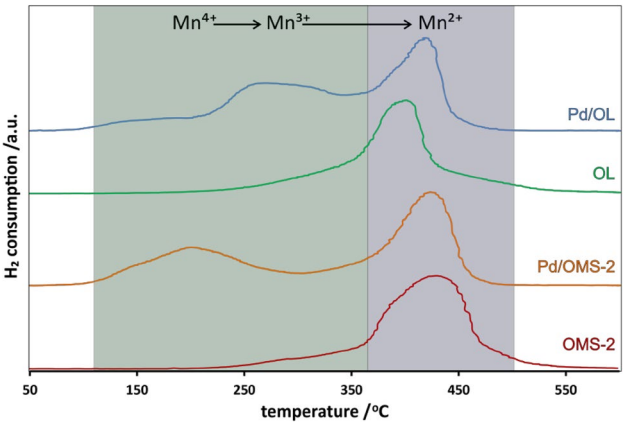

Fig. 4 TPR-H_2 of tested Pd-doped and undoped OL and OMS-2 catalysts

Pd supported catalysts. For Pd/OMS-2 the low temperature reduction is shifted down to 75–300 °C, while the second remains in the 300–500 °C range. In the case of Pd/OL the low temperature peak occurs in the 230–340 °C range, while the high temperature one is shifted to a higher range of 340–480 °C, the higher range being similar to the second reduction peak of OMS-2, once again showing the partial transformation to OMS-2. The low temperature reduction most likely occurs due to the hydrogen activation and spillover effect, which is widely described for palladium nanoparticles.

From SEM and TEM images (Fig. 5.) we can see the well-defined nanorod structure of OMS-2 and Pd/OMS-2. While for OL the SEM and TEM images revealed the characteristic layered material of OL. SEM and TEM images of Pd/OL confirm the phase transition observed by XRD. The layered material of OL has underwent a phase transition, revealing a well-defined nanorods structure, characteristic morphology, shown by OMS-2 materials. XRD showed peaks corresponding to remaining OL in XRD pattern, this is also evident from SEM where layered material can also be observed alongside the nanorods. From SEM, TEM and XRD analysis we can confirm there is no structural change upon immobilization of Pd nanoparticles to OMS-2. The OMS-2 material is stable and remains unchanged with well-defined nanorods visible in both OMS-2 and Pd/OMS-2.

Results from the catalytic activity tests are shown in Fig. 6. As can be inferred from the shift in soot conversion curves, palladium promotion had a promotional effect on catalytic activity. This effect is observed for both OL and OMS-2 supports independently of the test conditions. However, the most pronounced effect is observed for loose contact conditions. Whereas in tight contact the addition of 1% Pd on manganese oxide lowered the soot oxidation temperature ($T_{50\%}$) by a mere 10 °C (OL) and 5 °C (OMS-2) in loose contact, the shift reaches 65 and 60 °C, respectively. The most essential results concern the addition of NO, greatly bridging the gap between *tight* and *loose* contact conditions. It is worth noting, that the lowering of the soot oxidation window in comparison to the uncatalyzed reaction is > 250 °C. The significance of these results is in achieving the thermal conditions relevant for soot combustion in the temperature of real Diesel exhaust gases. The observed activity of the catalysts is comparable or better than found in literature [24, 40, 41]. In all tested conditions Pd/OL was the most active catalyst, achieving 50% soot conversion at 385, 450 and 541 °C for *tight, loose* + NO and *loose* contact conditions.

4 Conclusions

The paper presents comprehensive studies concerning the synergistic effects in catalytic soot oxidation between the potassium containing manganese oxides and palladium nanoparticles. The research presented in the paper reveals evidence of strong metal-support interaction leading to a partial phase transition upon 1% Pd decoration of OL, while the OMS-2 structure remains intact. The results show the highly beneficial effect of palladium on the catalytic activity

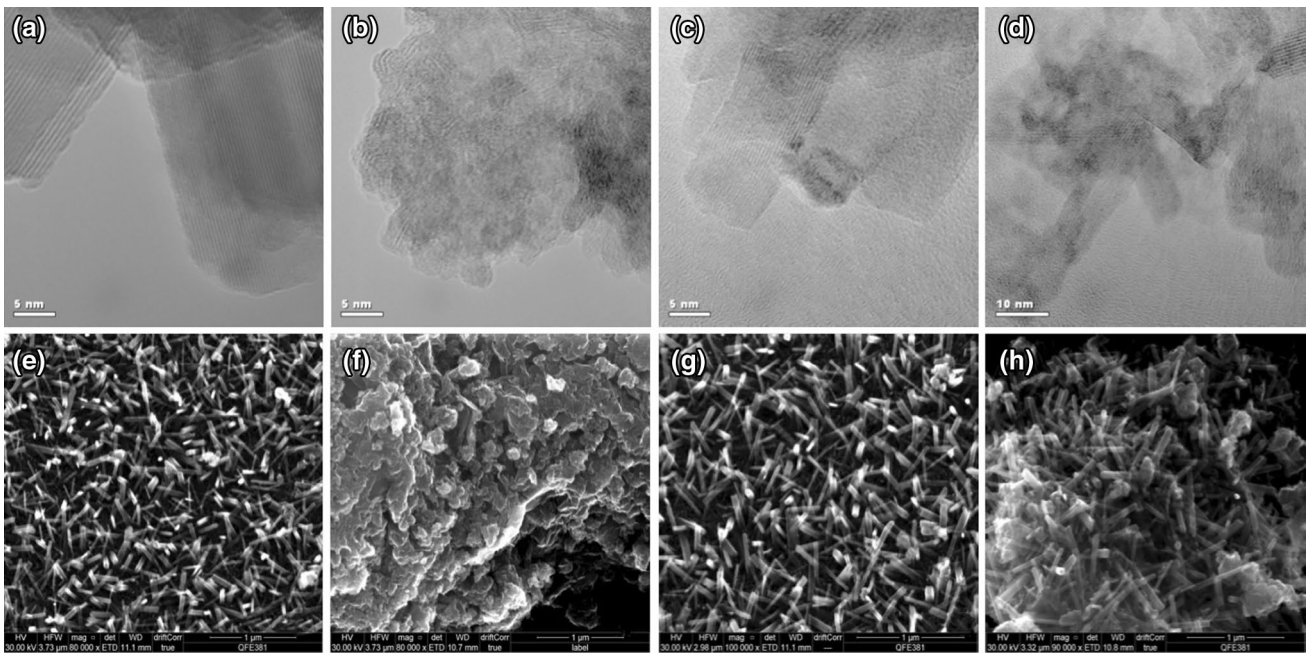

Fig. 5 TEM images of **a** OMS-2, **b** OL, **c** Pd/OMS-2, **d** Pd/OL and SEM images of **e** OMS-2, **f** OL, **g** Pd/OMS-2, **h** Pd/OL

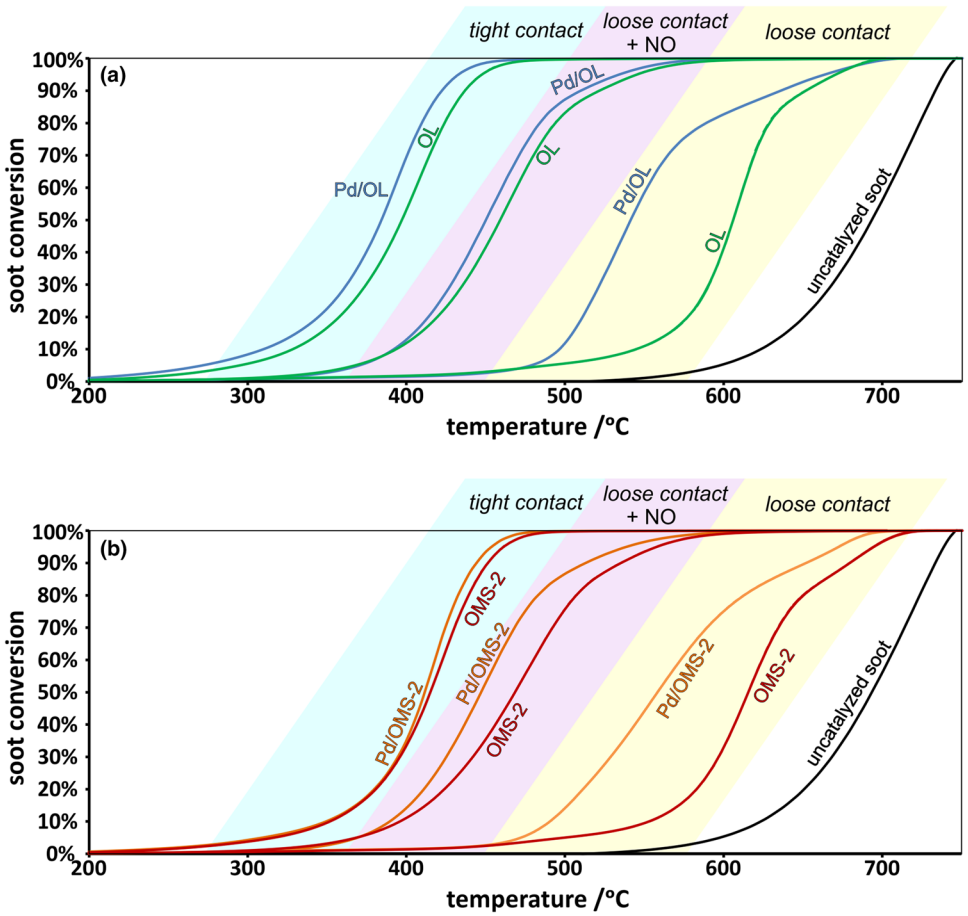

Fig. 6 Results of soot combustion tests of Pd-doped and undoped OL and OMS-2 catalysts in *loose* and *tight* contact without and with NO addition

of the two supports, especially in more realistic *loose* contact conditions, increasing the catalytic activity of the support in all cases. The 1% Pd surface promotion of OL is the most beneficial of the two. Compared to the non-catalytic soot combustion, the temperature of 50% soot conversion was shifted down by 315, 250 and 160 °C in *tight, loose* + NO and *loose* contact conditions, respectively, lowering the reaction window to temperatures relevant for soot combustion in Diesel exhaust engines.

Acknowledgements The study was supported by the Polish National Science Centre project awarded by decision number UMO-2017/24/T/ST5/00413.

Compliance with Ethical Standards

Conflict of interest The authors declare no conflict of interest.

References

1. Naapen AMK, Orm PJAB, Lbrecht CA, Chins RPFS (2004) Int J Cancer 109:799
2. Jacobson MZ (2001) Nature 409:695
3. Fino D (2007) Sci Technol Adv Mater 8:93
4. Van Setten BAAL, Schouten JM, Makkee M, Moulijn JA (2000) Catal Rev 28:253
5. Atribak I, Such-Basáñez I, Bueno-López A, García-García A (2007) J Catal 250:75
6. Wagloehner S, Baer JN, Kureti S (2014) Appl Catal B Environ 147:1000
7. Shen Q, Wu M, Wang H, He C, Hao Z, Wei W, Sun Y (2015) Catal Sci Technol 5:1941
8. Chen DL, Pan KL, Chang MB (2016) J Environ Sci 56:131–139
9. Dai F, Yu Y, Meng M, Zhang J, Zheng L, Hu T (2014) Catal Lett 144:1210
10. Zawadzki M, Walerczyk W, López-Suárez FE, Illán-Gómez MJ, Bueno-López A (2011) Catal Commun 12:1238
11. Wang J, Yang G, Cheng L (2015) Catal Sci Technol 5:4594
12. Mishra A, Prasad R (2014) Catal Rev 56:57
13. Fino D, Cauda E, Mescia D, Russo N, Saracco G, Specchia V (2007) Catal Today 119:257
14. Bueno-López A, Krishna K, van der Linden B, Mul G, Moulijn JA, Makkee M (2007) Catal Today 121:237
15. Bueno-López A (2014) Appl Catal B Environ 146:1
16. Hernández-Giménez AM, Castelló DL, Bueno-López A (2014) Chem Pap 68:1154

17. Mizutani K, Takizawa K, Shimokawa H, Suzawa T, Ohyama N (2013) Top Catal 56:473
18. Legutko P, Stelmachowski P, Trębala M, Sojka Z, Kotarba A (2013) Top Catal 56:489
19. Legutko P, Jakubek T, Kaspera W, Stelmachowski P, Sojka Z, Kotarba A (2014) Catal Commun 43:34
20. Tikhomirov K, Kröcher O, Wokaun A (2006) Catal Lett 109:49
21. Legutko P, Jakubek T, Kaspera W, Stelmachowski P, Sojka Z, Kotarba A (2016) Top Catal 60:162–170
22. Legutko P, Kaspera W, Stelmachowski P, Sojka Z, Kotarba A (2014) Catal Commun 56:139
23. Luo J, Zhang Q, Garcia-Martinez J, Suib SL (2008) J Am Chem Soc 130:3198
24. Atribak I, Bueno-López A, García-García A, Navarro P, Frías D, Montes M (2010) Appl Catal B Environ 93:267
25. Davo-Quinonero A, Navlani-Garcia M, Lozano-Castello D, Bueno-Lopez A (2016) Catal Sci Technol 6:5684
26. Yadav GD, Manyar HG (2008) Adv Synth Catal 350:2286
27. Ching S, Driscoll PF, Kieltyka KS, Marvel MR, Suib SL (2001) Chem Commun 23:2486
28. Hou J, Li Y, Mao M, Ren L, Zhao X (2014) ACS Appl Mater Interfaces 6:14981
29. Santos VP, Pereira MFR, Órfão JJM, Figueiredo JL (2010) Appl Catal B Environ 99:353
30. Peluso MA, Gambaro LA, Pronsato E, Gazzoli D, Thomas HJ, Sambeth JE (2008) Catal Today 133–135:487
31. Holmlid L (2002) J Phys Condens Matter 14:13469
32. Stelmachowski P, Legutko P, Jakubek T, Indyka P, Sojka Z, Holmlid L, Kotarba A (2015) Phys Chem Chem Phys 17:26289
33. Duan N, Suib SL, O'Young CL (1995) J Chem Soc Chem Commun 13:1367
34. Gao Q, Giraldo O, Tong W, Suib SL (2001) Chem Mater 13:778
35. Julien A, Massot M, Baddour-hadjean R, Franger S, Bach S, Pereira-ramos JP (2003) Solid State Ionics 159:345
36. El-sawy AM, Dutta PK, Suib SL (2012) J Phys Chem C 116:6474
37. Gao T, Glerup M, Krumeich F, Nesper R, Fjellvâg H, Norby P (2008) J Phys Chem C 112:13134
38. Figueira BAM, Angélica RS, da Costa ML, Pöllmann H, Schenzel K (2013) Appl Clay Sci 86:54
39. Liu X, Jin Z, Lu J, Wang X, Luo M (2010) Chem Eng J 162:151
40. Becerra M, Arias N, Giraldo O, Bueno-lópez A (2012) Catalysts 2:352
41. Li Q, Wang X, Chen H, Xin Y, Tian G, Lu C, Zhang Z, Zheng L, Zheng L (2016) Catal Today 264:171

Affiliations

Tomasz Jakubek[1] · Kathryn Ralphs[2] · Andrzej Kotarba[1] · Haresh Manyar[2]

[1] Faculty of Chemistry, Jagiellonian University, Kraków, Poland

[2] Theoretical and Applied Catalysis cluster, School of Chemistry and Chemical Engineering, Queen's University Belfast, David-Kier Building, Stranmillis Road, Belfast BT9 5AG, UK